L. Dozio
Exact Free Vibration Analysis of Lévy FGM Plates with Higher-Order Shear and Normal Deformation Theories
Composite Structures, Vol. 111, 2014, p. 415-425
doi:10.1016/j.compstruct.2014.01.014

Exact free vibration analysis of Lévy FGM plates with higher-order shear and normal deformation theories

Lorenzo Dozio

Department of Aerospace Science and Technology, Politecnico di Milano, via La Masa, 34, 20156, Milano, Italy

Abstract

First-known exact solutions are derived for free vibration of thick and moderately thick functionally graded rectangular plates with at least one pair of opposite edges simply-supported on the basis of a family of two-dimensional shear and normal deformation theories with variable order. The boundary-value problem is first expressed in a compact unified form which is invariant with respect to the order of the kinematic theory. The Lévy method applied to this compact form yields a set of governing equations written in terms of invariant matrices, which are then appropriately expanded according to the order of the plate model. The resulting equations are put into a state-space representation and the frequency values are finally obtained by substituting the general solution of the state equation into the set of boundary conditions and solving the related homogeneous system. After discussing the way of recovering the through-the-thickness modal displacement and stress distribution at any point of the plate and how the effective elastic properties of the graded plate are computed, some numerical results are presented using various higher-order theories. Comparisons with exact three-dimensional and other two-dimensional approaches are provided for two-constituents metal-ceramic plates. New exact results for functionally graded plates with six combinations of boundary conditions are also obtained. They can be useful as valuable sources for validating other approaches and approximate methods.

Key words: Free vibration, exact solutions, Lévy plates, functionally graded material, higher-order plate theories.

1. Introduction

Functionally graded materials (FGMs) are receiving increasing attention in recent years since they offer great promise in many engineering applications. For example, due to their smooth spatial variation of material properties, they are attractive for advanced thermal barrier coatings in engine components and spacecraft heat shields. Conventional thermal barrier systems consisting of a discrete layer of ceramic

Email address: lorenzo.dozio@polimi.it (Lorenzo Dozio)

material bonded to a metallic structure could be replaced by a FGM structure with ceramic-rich material placed at the high temperature regions and metal-rich material located where high mechanical properties are needed. By doing so, large interlaminar stresses originating at the interface between distinct materials could be avoided.

The above mentioned interest motivated a huge amount of research in the characterization, modelling and analysis of FGM structures, with particular attention to plates and shells. An extensive literature review on FGM plates has been recently provided by Jha et al. [1], with a strong emphasis on available methods of estimating effective properties of FGMs and on thermo-elastic, vibration and stability analysis. Since more than 190 works published since 1998 are critically examined and classified, interested readers are warmly referred to [1] for a comprehensive overview of ongoing research on functionally graded plates.

Generally speaking, recent studies on FGM plates are focused on three main topics: homogenization models and schemes to simplify FGM complicated heterogeneous microstructures, kinematic models to accurately describe the mechanical behavior of plates made of FGM, and solution techniques to provide numerical evaluation of their static and dynamic response. This work addresses the second and third topic by presenting the first-known exact vibration solutions of rectangular FGM plates having at least two opposite edges simply-supported on the basis of a family of two-dimensional (2-D) theories with shear and normal deformation effects. Effective elastic properties of the FGM plate are computed by means of the classical rule-of-mixtures or the Mori-Tanaka homogenization scheme [2], as explained later.

It is well known that exact analysis of structural elements is relevant in providing valuable comparison to study convergence and accuracy of approximate solution methods. In addition, analytical models may be highly appealing to speed up the preliminary structural design when many parametric and optimization studies are carried out. Exact solutions for free vibrations of plates are only available for a limited set of geometrical and material configurations. The case under study in this work belongs to that set and involves a rectangular plate having FGM properties varying smoothly through the thickness and with one pair of opposite edges simply-supported and the remaining edges having any combination of free, simple support or clamped conditions. Rectangular plates with at least two opposite edges simply-supported are often denoted in the literature as Lévy plates since they can be analyzed by employing the so-called Lévy solution method. Lévy developed in 1899 an exact method for bending analysis of isotropic rectangular plates based on the expansion of the displacement field in a single trigonometric series along the direction normal to the pair of opposite simply-supported edges. The same approach can be applied as well to specially orthotropic and FGM plates and to dynamic problems. It is noted that the method was actually introduced by Voigt for solving the free vibration problem of isotropic plates six years before Lévy published his work on bending analysis [3].

Exact vibration solutions of FGM plates are rather limited in the open literature. A remarkable three-dimensional (3-D) exact solution is presented by Vel and Batra [4]. Free and forced vibrations of thin and

thick simply-supported plates with arbitrary variation of material properties in the thickness direction are studied. Benchmark values are obtained from 3-D elasticity for two-constituents metal-ceramic FG plates and used to assess the accuracy of the classical plate theory (CPT) and the first-order shear deformation theory (FOST). It is shown that both theories may be inadequate for FGM plates since CPT completely neglects the effects of transverse shear strains and FOST solutions are strongly dependent on the estimates of the shear correction factor.

In order to overcome the limitations of traditional theories, many higher-order theories have been proposed in the literature with the aim of providing accurate 2-D models without the need of a cumbersome full 3-D analysis. Higher-order 2-D plate models can be considered as refinements of FOST, where the assumed displacement field of FOST is typically enriched with higher-order terms as Taylor's series expansion of the thickness coordinate. The highest power in the Taylor's expansion is denoted as order of the theory. It is possible to distinguish between higher-order shear deformation theories (HOSTs), where in-plane displacements are assumed to be at least a parabolic expression of the thickness coordinate and the out-of-plane displacement to be constant, and higher-order shear and normal deformation theories (HOSNTs), where thickness stretching is allowed by including also power series expansion of the transverse displacement. Two excellent examples of application of higher-order theories to FGM plates are proposed by Matsunaga [5] and Jha et al. [6]. Matsunaga [5] investigates a general 2-D HOSNT which takes into account the effects of shear deformations, transverse extensibility and rotary inertia. Exact free vibration and stability analysis of rectangular fully simply-supported FG metal-ceramic plates is performed by the Navier method. It is shown by comparison with 3-D results that HOSNTs can provide accurate solutions both for frequency values and buckling stresses. Jha et al. [6] present a comprehensive study of shear deformation theories of different order with and without normal deformation effects for free vibration analysis of FGM plates. The analysis is limited to Navier solution for plates with all edges simply-supported. It is shown through many numerical examples that HOSNTs are required to achieve the accuracy of 3-D elasticity solutions, especially when the side-to-thickness ratio of the plate is less than 10.

Papers on exact vibration analysis of rectangular FGM plates with boundary conditions other than all simply-supported are very few. Thin functionally graded plates are considered by Hasani Baferani et al. [7]. Both Navier and Lévy-type solutions are obtained based on the classical plate theory and the effects of boundary conditions on the vibration characteristics are discussed. An exact closed-form solution is presented by Hosseini-Hashemi et al. [8] for moderately thick Lévy FGM plates. The analysis is performed using the first-order shear deformation theory with a shear correction factor taken as 5/6 and numerical results are presented for six different combinations of boundary conditions. The same authors report a study in Ref. [9] where an exact analytical vibration solution of thick FGM plates is derived on the basis of the third-order shear deformation theory proposed by Reddy [10]. In this way, no shear correction factor is needed. It is shown that the Reddy's model yields a slightly improved accuracy with respect to FOST.

Hasani Baferani et al. [11] use the same third-order plate model to present Lévy-type solutions of rectangular FGM plates resting on elastic foundation.

From the previous review, it is evident the lack of exact solutions of Lévy FGM plates based on HOSNTs. This is probably due to the mathematical complexity of the problem, which is related to the coupling between in-plane and out-of-plane motion induced by the through-the-thickness variation of elastic properties and the number of highly-coupled differential equations of motions arising from the relatively high number of kinematic variables in the assumed displacement field. Moreover, all previous approaches rely on governing equations and solution procedures which are specific to the particular plate theory adopted. Therefore, if the theory is changed, the mathematical formulation and, in some cases, the corresponding solution technique should be adapted accordingly.

The aim of this work is to present a powerful unified approach capable of providing in an easy and automatic way exact vibration solutions of Lévy FGM plates on the basis of an entire family of HOSNTs with variable order. The formulation here proposed can be considered as an extension to FGM plates of what recently presented in Ref. [12] for laminated plates. As shown in Section 2, by writing the assumed plate model using an index notation related to the order of expansion of in-plane and out-of-plane displacements, the equations of motion and boundary conditions can be expressed in a compact form which is invariant with respect to the order of the kinematic theory. Section 3 shows how the Lévy method applied to the previous form yields a set of governing equations written in terms of 3×3 matrices, called *fundamental nuclei* of the formulation, which again do not depend on the order of the theory. The nuclei are then appropriately expanded according to the order of the plate model and the resulting equations are put into a first-order state-space representation. The frequency values are finally obtained by substituting the general solution of the state equation into the set of boundary conditions and solving the related homogeneous system. After discussing the way of recovering the through-the-thickness modal displacement and stress distribution at any point of the plate and how the effective elastic properties of the graded plate are computed, some numerical results are presented in Section 6 using various HOSNTs. Comparisons with exact 3-D and other 2-D approaches are provided for two-constituents metal-ceramic plates with various boundary conditions along with new exact results which can serve as benchmark cases for approximate methods.

2. The boundary-value problem

Consider a rectangular plate of length a, width b and uniform thickness h in the unstressed reference configuration. The plate is made of elastic and isotropic functionally graded material with properties varying smoothly in the z thickness direction only. In the absence of external forces, the principle of virtual

displacements (PVD) may be written as follows

$$\int_{\Omega}\int_{-h/2}^{h/2}\left(\delta\boldsymbol{\epsilon}_{\rm p}^{\rm T}\boldsymbol{\sigma}_{\rm p}+\delta\boldsymbol{\epsilon}_{\rm n}^{\rm T}\boldsymbol{\sigma}_{\rm n}\right)\mathrm{d}z\mathrm{d}\Omega=-\int_{\Omega}\int_{-h/2}^{h/2}\delta\mathbf{u}^{\rm T}\rho(z)\frac{\partial^2\mathbf{u}}{\partial t^2}\mathrm{d}z\mathrm{d}\Omega \tag{1}$$

where

$$\mathbf{u}(x,y,z,t)=\left[\begin{array}{ccc} u(x,y,z,t) & v(x,y,z,t) & w(x,y,z,t)\end{array}\right]^{\rm T} \tag{2}$$

is the displacement vector at any point (x,y,z) of the plate, $\Omega=[0,a]\times[0,b]$ is the middle surface, $\rho(z)$ is the mass density, and the stress and strain vectors are partitioned into in-plane and out-of-plane (normal) components as follows

$$\boldsymbol{\sigma}_{\rm p}=\left[\begin{array}{ccc}\sigma_{xx} & \sigma_{yy} & \tau_{xy}\end{array}\right]^{\rm T},\qquad \boldsymbol{\epsilon}_{\rm p}=\left[\begin{array}{ccc}\epsilon_{xx} & \epsilon_{yy} & \gamma_{xy}\end{array}\right]^{\rm T}$$
$$\boldsymbol{\sigma}_{\rm n}=\left[\begin{array}{ccc}\tau_{xz} & \tau_{yz} & \sigma_{zz}\end{array}\right]^{\rm T},\qquad \boldsymbol{\epsilon}_{\rm n}=\left[\begin{array}{ccc}\gamma_{xz} & \gamma_{yz} & \epsilon_{zz}\end{array}\right]^{\rm T}$$

The linear strain-displacements relations are expressed in matrix notation as

$$\boldsymbol{\epsilon}_{\rm p}=\boldsymbol{\mathcal{D}}_{\rm p}\mathbf{u},\qquad\qquad \boldsymbol{\epsilon}_{\rm n}=\boldsymbol{\mathcal{D}}_{\rm n}\mathbf{u}+\frac{\partial}{\partial z}\mathbf{u} \tag{3}$$

where

$$\boldsymbol{\mathcal{D}}_{\rm p}=\left[\begin{array}{ccc}\partial/\partial x & 0 & 0\\ 0 & \partial/\partial y & 0\\ \partial/\partial y & \partial/\partial x & 0\end{array}\right],\qquad\qquad \boldsymbol{\mathcal{D}}_{\rm n}=\left[\begin{array}{ccc}0 & 0 & \partial/\partial x\\ 0 & 0 & \partial/\partial y\\ 0 & 0 & 0\end{array}\right]$$

A family of 2-D higher-order shear and normal deformation plate theories is introduced as follows

$$\begin{aligned}\mathbf{u}(x,y,z,t)&=F_0(z)\mathbf{u}_0(x,y,t)+\cdots+F_N(z)\mathbf{u}_N(x,y,t)\\ &=F_\tau(z)\mathbf{u}_\tau(x,y,t)\end{aligned} \tag{4}$$

where $\tau=0,1,2,\ldots,N$ is the theory-related index, $F_\tau(z)$ are appropriate thickness functions, and

$$\mathbf{u}_\tau(x,y,t)=\left[\begin{array}{ccc}u_\tau(x,y,t) & v_\tau(x,y,t) & w_\tau(x,y,t)\end{array}\right]^{\rm T} \tag{5}$$

is the vector of generalized kinematic coordinates in the assumed displacement model. Note that in Eq. (4) the Einstein convention is used with an implied summation over the index τ. Note also that normal deformation effects are allowed by the expansion of the transverse displacement w. Various theories of different order can be obtained by selecting N and the type of thickness functions. Specific theories will be considered later in Section 6 where the numerical analysis is presented. The mathematical formulation is derived in the following be referring to the general case expressed by Eq. (4).

Substituting Eq. (4) into the strain-displacement relations (3) and the PVD equation (1) yields

$$\begin{aligned}&\int_{\Omega}\left[\left(\boldsymbol{\mathcal{D}}_{\rm p}\delta\mathbf{u}_\tau\right)^{\rm T}\boldsymbol{\mathcal{R}}_{{\rm p}\tau}+\left(\boldsymbol{\mathcal{D}}_{\rm n}\delta\mathbf{u}_\tau\right)^{\rm T}\boldsymbol{\mathcal{R}}_{{\rm n}\tau}+\delta\mathbf{u}_\tau^{\rm T}\boldsymbol{\mathcal{R}}_{{\rm n}\tau_z}\right]\mathrm{d}\Omega=\\ &-\int_{\Omega}\delta\mathbf{u}_\tau^{\rm T}\mathcal{I}_{\rho\tau s}\frac{\partial^2\mathbf{u}_s}{\partial t^2}\mathrm{d}\Omega\end{aligned} \tag{6}$$

which holds for any τ and s ranging from 0 to N. In the above equilibrium equation, the following stress resultants are introduced

$$\boldsymbol{\mathcal{R}}_{\mathrm{p}\tau} = \left\{ \begin{array}{c} \mathcal{R}_{xx\tau} \\ \mathcal{R}_{yy\tau} \\ \mathcal{R}_{xy\tau} \end{array} \right\} = \int_{-h/2}^{h/2} F_\tau \boldsymbol{\sigma}_{\mathrm{p}} \mathrm{d}z \tag{7}$$

$$\boldsymbol{\mathcal{R}}_{\mathrm{n}\tau} = \left\{ \begin{array}{c} \mathcal{R}_{xz\tau} \\ \mathcal{R}_{yz\tau} \\ \mathcal{R}_{zz\tau} \end{array} \right\} = \int_{-h/2}^{h/2} F_\tau \boldsymbol{\sigma}_{\mathrm{n}} \mathrm{d}z \tag{8}$$

$$\boldsymbol{\mathcal{R}}_{\mathrm{n}\tau_z} = \left\{ \begin{array}{c} \mathcal{R}_{xz\tau_z} \\ \mathcal{R}_{yz\tau_z} \\ \mathcal{R}_{zz\tau_z} \end{array} \right\} = \int_{-h/2}^{h/2} \frac{\mathrm{d}F_\tau}{\mathrm{d}z} \boldsymbol{\sigma}_{\mathrm{n}} \mathrm{d}z \tag{9}$$

and the thickness integrals $\mathcal{I}_{\rho\tau s}$ is defined as

$$\mathcal{I}_{\rho\tau s} = \int_{-h/2}^{h/2} \rho(z) F_\tau F_s \mathrm{d}z \tag{10}$$

After integrating by parts Eq. (6) and exploiting the arbitrariness of $\delta\mathbf{u}_\tau$ over the plate domain Ω, the equations of motion can be written in terms of stress resultants as

$$\begin{aligned} \delta u_\tau : \quad & \frac{\partial \mathcal{R}_{xx\tau}}{\partial x} + \frac{\partial \mathcal{R}_{xy\tau}}{\partial y} - \mathcal{R}_{xz\tau_z} = \mathcal{I}_{\rho\tau s} \frac{\partial^2 u_s}{\partial t^2} \\ \delta v_\tau : \quad & \frac{\partial \mathcal{R}_{xy\tau}}{\partial x} + \frac{\partial \mathcal{R}_{yy\tau}}{\partial y} - \mathcal{R}_{yz\tau_z} = \mathcal{I}_{\rho\tau s} \frac{\partial^2 v_s}{\partial t^2} \\ \delta w_\tau : \quad & \frac{\partial \mathcal{R}_{xz\tau}}{\partial x} + \frac{\partial \mathcal{R}_{yz\tau}}{\partial y} - \mathcal{R}_{zz\tau_z} = \mathcal{I}_{\rho\tau s} \frac{\partial^2 w_s}{\partial t^2} \end{aligned} \tag{11}$$

for $s = 0, 1, \ldots, N$. It is worth noting that, according to the compact index notation introduced above, three equations of the form (11) are written for each index τ leading to a system of $3(N+1)$ equations of motion. Using the summation convention over the index s, each equation contains $(N+1)$ inertial terms in the right-hand side. From the boundary terms arising from integration by parts of Eq. (6), the following geometric and equilibrium conditions along plate edges are obtained

$$\text{along } x = 0, a \qquad \left\{ \begin{array}{lll} u_\tau = 0 & \text{or} & \mathcal{R}_{xx\tau} = 0 \\ v_\tau = 0 & \text{or} & \mathcal{R}_{xy\tau} = 0 \\ w_\tau = 0 & \text{or} & \mathcal{R}_{xz\tau} = 0 \end{array} \right. \tag{12}$$

$$\text{along } y = 0, b \qquad \left\{ \begin{array}{lll} u_\tau = 0 & \text{or} & \mathcal{R}_{xy\tau} = 0 \\ v_\tau = 0 & \text{or} & \mathcal{R}_{yy\tau} = 0 \\ w_\tau = 0 & \text{or} & \mathcal{R}_{yz\tau} = 0 \end{array} \right. \tag{13}$$

Note again that Eqs. (12) and (13) are written for each value of index τ.

The constitutive equation of an isotropic FG material with varying properties along the thickness direction may be written as

$$\begin{aligned} \boldsymbol{\sigma}_{\mathrm{p}} &= \mathbf{C}_{\mathrm{pp}}(z)\boldsymbol{\epsilon}_{\mathrm{p}} + \mathbf{C}_{\mathrm{pn}}(z)\boldsymbol{\epsilon}_{\mathrm{n}} \\ \boldsymbol{\sigma}_{\mathrm{n}} &= \mathbf{C}^{\mathrm{T}}_{\mathrm{pn}}(z)\boldsymbol{\epsilon}_{\mathrm{p}} + \mathbf{C}_{\mathrm{nn}}(z)\boldsymbol{\epsilon}_{\mathrm{n}} \end{aligned} \tag{14}$$

where the matrices of stiffness coefficients are given by

$$\mathbf{C}_{\mathrm{pp}}(z) = \begin{bmatrix} C_{11}(z) & C_{12}(z) & 0 \\ C_{12}(z) & C_{22}(z) & 0 \\ 0 & 0 & C_{66}(z) \end{bmatrix} \tag{15}$$

$$\mathbf{C}_{\mathrm{pn}}(z) = \begin{bmatrix} 0 & 0 & C_{13}(z) \\ 0 & 0 & C_{23}(z) \\ 0 & 0 & 0 \end{bmatrix} \tag{16}$$

$$\mathbf{C}_{\mathrm{nn}}(z) = \begin{bmatrix} C_{55}(z) & 0 & 0 \\ 0 & C_{44}(z) & 0 \\ 0 & 0 & C_{33}(z) \end{bmatrix} \tag{17}$$

and

$$\begin{aligned} C_{11} = C_{22} = C_{33} &= \frac{E(z)\left[1-\nu(z)\right]}{\left[1+\nu(z)\right]\left[1-2\nu(z)\right]} \\ C_{12} = C_{13} = C_{23} &= \frac{E(z)\nu(z)}{\left[1+\nu(z)\right]\left[1-2\nu(z)\right]} \\ C_{44} = C_{55} = C_{66} &= \frac{E(z)}{2\left[1+\nu(z)\right]} \end{aligned} \tag{18}$$

in which $E(z)$ and $\nu(z)$ are, respectively, the Young's modulus and Poisson's ratio as a function of the thickness coordinate. Methods used in this work to estimate them are presented in Section 5.

By inserting Eq. (14) into Eqs. (7-9) and using again the strain-displacement relations, the equations of motion expressed in Eq. (11) for each index τ can be compactly written in terms of displacement coordinates

as follows

$$\begin{aligned}
&\left[\mathcal{I}^{00}_{11\tau s}\frac{\partial^2}{\partial x^2}+\mathcal{I}^{00}_{66\tau s}\frac{\partial^2}{\partial y^2}-\mathcal{I}^{11}_{55\tau s}\right]u_s+\left(\mathcal{I}^{00}_{12\tau s}+\mathcal{I}^{00}_{66\tau s}\right)\frac{\partial^2 v_s}{\partial x\partial y}\\
&\quad+\left(\mathcal{I}^{01}_{13\tau s}-\mathcal{I}^{10}_{55\tau s}\right)\frac{\partial w_s}{\partial x}=\mathcal{I}_{\rho\tau s}\frac{\partial^2 u_s}{\partial t^2}\\
&\left(\mathcal{I}^{00}_{12\tau s}+\mathcal{I}^{00}_{66\tau s}\right)\frac{\partial^2 u_s}{\partial y\partial x}+\left[\mathcal{I}^{00}_{66\tau s}\frac{\partial^2}{\partial x^2}+\mathcal{I}^{00}_{22\tau s}\frac{\partial^2}{\partial y^2}-\mathcal{I}^{11}_{44\tau s}\right]v_s\\
&\quad+\left(\mathcal{I}^{01}_{23\tau s}-\mathcal{I}^{10}_{44\tau s}\right)\frac{\partial w_s}{\partial y}=\mathcal{I}_{\rho\tau s}\frac{\partial^2 v_s}{\partial t^2}\\
&\left(\mathcal{I}^{01}_{55\tau s}-\mathcal{I}^{10}_{13\tau s}\right)\frac{\partial u_s}{\partial x}+\left(\mathcal{I}^{01}_{44\tau s}-\mathcal{I}^{10}_{23\tau s}\right)\frac{\partial v_s}{\partial y}\\
&\quad+\left[\mathcal{I}^{00}_{55\tau s}\frac{\partial^2}{\partial x^2}+\mathcal{I}^{00}_{44\tau s}\frac{\partial^2}{\partial y^2}-\mathcal{I}^{11}_{33\tau s}\right]w_s=\mathcal{I}_{\rho\tau s}\frac{\partial^2 w_s}{\partial t^2}
\end{aligned}\tag{19}$$

where

$$\mathcal{I}^{\alpha\beta}_{ij\tau s}=\int_{-h/2}^{h/2}C_{ij}(z)\frac{\mathrm{d}^\alpha F_\tau}{\mathrm{d}z^\alpha}\frac{\mathrm{d}^\beta F_s}{\mathrm{d}z^\beta}\mathrm{d}z \tag{20}$$

are thickness integrals involving the stiffness material properties.

Accordingly, the boundary conditions along $x=0,a$ can be written as

$$\begin{cases}
u_\tau=0 \quad \text{or} \quad \mathcal{I}^{00}_{11\tau s}\dfrac{\partial u_s}{\partial x}+\mathcal{I}^{00}_{12\tau s}\dfrac{\partial v_s}{\partial y}+\mathcal{I}^{01}_{13\tau s}w_s=0\\
v_\tau=0 \quad \text{or} \quad \mathcal{I}^{00}_{66\tau s}\left(\dfrac{\partial u_s}{\partial y}+\dfrac{\partial v_s}{\partial x}\right)=0\\
w_\tau=0 \quad \text{or} \quad \mathcal{I}^{01}_{55\tau s}u_s+\mathcal{I}^{00}_{55\tau s}\dfrac{\partial w_s}{\partial x}=0
\end{cases}\tag{21}$$

and along $y=0,b$ as

$$\begin{cases}
u_\tau=0 \quad \text{or} \quad \mathcal{I}^{00}_{66\tau s}\left(\dfrac{\partial u_s}{\partial y}+\dfrac{\partial v_s}{\partial x}\right)=0\\
v_\tau=0 \quad \text{or} \quad \mathcal{I}^{00}_{12\tau s}\dfrac{\partial u_s}{\partial x}+\mathcal{I}^{00}_{22\tau s}\dfrac{\partial v_s}{\partial y}+\mathcal{I}^{01}_{23\tau s}w_s=0\\
w_\tau=0 \quad \text{or} \quad \mathcal{I}^{01}_{44\tau s}v_s+\mathcal{I}^{00}_{44\tau s}\dfrac{\partial w_s}{\partial y}=0
\end{cases}\tag{22}$$

3. Exact solution

Exact Lévy-type solutions of the boundary-value problem described by Eqs. (19), (21) and (22) can be obtained if the plate is at least simply-supported at two opposite edges. Without any loss of generality, let consider the FGM plate being simply supported at $y=0$ and $y=b$. The edges at $x=0$ and $x=a$ may be free, simply-supported or clamped. The condition of simple support along one edge is specified herein as null tangential and transverse displacements and null normal stress. Therefore, according to what derived

in the previous section, the displacement field must satisfy the following equations

$$\begin{aligned} & u_\tau = 0 \\ & \mathcal{I}^{00}_{12\tau s}\frac{\partial u_s}{\partial x} + \mathcal{I}^{00}_{22\tau s}\frac{\partial v_s}{\partial y} + \mathcal{I}^{01}_{23\tau s} w_s = 0 \\ & w_\tau = 0 \end{aligned} \tag{23}$$

along $y = 0$ and $y = b$ for any theory-related index $\tau, s = 0, \ldots, N$. A solution for free harmonic motion of the FGM plate satisfying the above boundary conditions is sought in the following form

$$\mathbf{u}_s = \left\{ \begin{array}{l} u_{sm}(x)\sin(\beta_m y) \\ v_{sm}(x)\cos(\beta_m y) \\ w_{sm}(x)\sin(\beta_m y) \end{array} \right\} e^{j\omega_m t} \qquad (m = 1, 2, \ldots) \tag{24}$$

where ω_m denotes the unknown eigenfrequency corresponding to m and $\beta_m = m\pi/b$. Substituting the Lévy-type solution (24) into Eqs. (19) yields the following system of second-order ordinary differential equations

$$\mathbf{L}^{\tau s}_2 \frac{\mathrm{d}^2 \mathbf{u}_{sm}}{\mathrm{d}x^2} - \mathbf{L}^{\tau s}_1 \frac{\mathrm{d}\mathbf{u}_{sm}}{\mathrm{d}x} - \mathbf{L}^{\tau s}_0 \mathbf{u}_{sm} = \mathbf{0} \qquad (m = 1, 2, \ldots) \tag{25}$$

where

$$\mathbf{u}_{sm}(x) = \left[\begin{array}{ccc} u_{sm}(x) & v_{sm}(x) & w_{sm}(x) \end{array} \right]^{\mathrm{T}} \tag{26}$$

is the vector of unknown amplitudes and

$$\mathbf{L}^{\tau s}_2 = \left[\begin{array}{ccc} \mathcal{I}^{00}_{11\tau s} & 0 & 0 \\ 0 & \mathcal{I}^{00}_{66\tau s} & 0 \\ 0 & 0 & \mathcal{I}^{00}_{55\tau s} \end{array} \right] \tag{27}$$

$$\mathbf{L}^{\tau s}_1 = \left[\begin{array}{ccc} 0 & \ell_{12} & \ell_{13} \\ \ell_{21} & 0 & 0 \\ \ell_{31} & 0 & 0 \end{array} \right] \tag{28}$$

$$\mathbf{L}^{\tau s}_0 = \left[\begin{array}{ccc} \ell_{11} & 0 & 0 \\ 0 & \ell_{22} & \ell_{23} \\ 0 & \ell_{32} & \ell_{33} \end{array} \right] \tag{29}$$

in which

$$
\begin{aligned}
\ell_{12} &= \beta_m \left(\mathcal{I}^{00}_{12\tau s} + \mathcal{I}^{00}_{66\tau s} \right) \\
\ell_{13} &= \left(\mathcal{I}^{10}_{55\tau s} - \mathcal{I}^{01}_{13\tau s} \right) \\
\ell_{21} &= -\beta_m \left(\mathcal{I}^{00}_{12\tau s} + \mathcal{I}^{00}_{66\tau s} \right) \\
\ell_{31} &= -\left(\mathcal{I}^{01}_{55\tau s} - \mathcal{I}^{10}_{13\tau s} \right) \\
\ell_{11} &= \beta_m^2 \mathcal{I}^{00}_{66\tau s} + \mathcal{I}^{11}_{55\tau s} - \mathcal{I}_{\rho\tau s}\omega_m^2 \\
\ell_{22} &= \beta_m^2 \mathcal{I}^{00}_{22\tau s} + \mathcal{I}^{11}_{44\tau s} - \mathcal{I}_{\rho\tau s}\omega_m^2 \\
\ell_{23} &= \beta_m \left(\mathcal{I}^{10}_{44\tau s} - \mathcal{I}^{01}_{23\tau s} \right) \\
\ell_{32} &= \beta_m \left(\mathcal{I}^{01}_{44\tau s} - \mathcal{I}^{10}_{23\tau s} \right) \\
\ell_{33} &= \beta_m^2 \mathcal{I}^{00}_{44\tau s} + \mathcal{I}^{11}_{33\tau s} - \mathcal{I}_{\rho\tau s}\omega_m^2
\end{aligned}
\tag{30}
$$

Note again that, similarly to Eq. (19), the differential equations (25) along x direction are written in compact notation for each pair (τ, s) and therefore they do not depend on the order N of the assumed plate theory. The same invariance property with respect to N holds for the corresponding 3×3 matrices $\mathbf{L}^{\tau s}_n$ $(n = 0, 1, 2)$, which are called, for this reason, *fundamental nuclei* of the formulation.

Doing the same for the boundary conditions at edges $x = 0$ and $x = a$, the following equations are obtained

$$
\begin{aligned}
&\mathbf{B}^{\tau s}_1 \frac{\mathrm{d}\mathbf{u}_{sm}}{\mathrm{d}x}(0) + \mathbf{B}^{\tau s}_0 \mathbf{u}_{sm}(0) = \mathbf{0} \\
&\mathbf{B}^{\tau s}_1 \frac{\mathrm{d}\mathbf{u}_{sm}}{\mathrm{d}x}(a) + \mathbf{B}^{\tau s}_0 \mathbf{u}_{sm}(a) = \mathbf{0}
\end{aligned}
\qquad (m = 1, 2, \dots)
\tag{31}
$$

where $\mathbf{B}^{\tau s}_n$ $(n = 0, 1)$ are the 3×3 *boundary-related fundamental nuclei* of the formulation. They are expressed according to the type of edge conditions at $x = 0$ and $x = a$. If the edge is clamped, the displacement field is enforced to be null. Therefore, $\mathbf{B}^{\tau s}_n$ reduce to

$$
\mathbf{B}^{\tau s}_1 = \mathbf{0}, \qquad \mathbf{B}^{\tau s}_0 = \mathbf{I}
\tag{32}
$$

For a free edge, natural boundary conditions of null stress resultants must be satisfied. Accordingly, the boundary-related nuclei are given by

$$
\begin{aligned}
\mathbf{B}^{\tau s}_1 &= \begin{bmatrix} \mathcal{I}^{00}_{11\tau s} & 0 & 0 \\ 0 & \mathcal{I}^{00}_{66\tau s} & 0 \\ 0 & 0 & \mathcal{I}^{00}_{55\tau s} \end{bmatrix} \\
\mathbf{B}^{\tau s}_0 &= \begin{bmatrix} 0 & -\beta_m \mathcal{I}^{00}_{12\tau s} & \mathcal{I}^{01}_{13\tau s} \\ \beta_m \mathcal{I}^{00}_{66\tau s} & 0 & 0 \\ \mathcal{I}^{01}_{55\tau s} & 0 & 0 \end{bmatrix}
\end{aligned}
\tag{33}
$$

Finally, a simply-supported edge at $x = 0$ or $x = a$ is represented by

$$\begin{aligned} \mathbf{B}_1^{\tau s} &= \begin{bmatrix} \mathcal{I}_{11\tau s}^{00} & 0 & 0 \\ 0 & 0 & 0 \\ 0 & 0 & 0 \end{bmatrix} \\ \mathbf{B}_0^{\tau s} &= \begin{bmatrix} 0 & -\beta_m \mathcal{I}_{12\tau s}^{00} & \mathcal{I}_{13\tau s}^{01} \\ 0 & 1 & 0 \\ 0 & 0 & 1 \end{bmatrix} \end{aligned} \tag{34}$$

As already stated, Equations (25) and (31) are written in terms of fundamental nuclei for each pair (τ, s). In order to obtain the governing equations and related boundary conditions of the FGM plate according to the assumed kinematic theory, a simple expansion procedure is applied. By varying the theory-related indices τ and s over the range $0, \ldots, N$, the nuclei are expanded so that a final system of equations and related boundary conditions for $m = 1, 2, \ldots$ is obtained as follows

$$\begin{cases} \mathbf{L}_2 \dfrac{\mathrm{d}^2 \mathbf{u}_m}{\mathrm{d}x^2} - \mathbf{L}_1 \dfrac{\mathrm{d}\mathbf{u}_m}{\mathrm{d}x} - \mathbf{L}_0 \mathbf{u}_m = \mathbf{0} \\ \\ \mathbf{B}_1 \dfrac{\mathrm{d}\mathbf{u}_m}{\mathrm{d}x}(0) + \mathbf{B}_0 \mathbf{u}_m(0) = \mathbf{0} \\ \\ \mathbf{B}_1 \dfrac{\mathrm{d}\mathbf{u}_m}{\mathrm{d}x}(a) + \mathbf{B}_0 \mathbf{u}_m(a) = \mathbf{0} \end{cases} \tag{35}$$

where

$$\begin{aligned} \mathbf{L}_n &= \begin{bmatrix} \mathbf{L}_n^{00} & \mathbf{L}_n^{01} & \ldots & \mathbf{L}_n^{0N} \\ \mathbf{L}_n^{10} & \mathbf{L}_n^{11} & \ldots & \mathbf{L}_n^{1N} \\ \vdots & & & \\ \mathbf{L}_n^{N0} & \mathbf{L}_n^{N1} & \ldots & \mathbf{L}_n^{NN} \end{bmatrix} \\ \mathbf{B}_n &= \begin{bmatrix} \mathbf{B}_n^{00} & \mathbf{B}_n^{01} & \ldots & \mathbf{B}_n^{0N} \\ \mathbf{B}_n^{10} & \mathbf{B}_n^{11} & \ldots & \mathbf{B}_n^{1N} \\ \vdots & & & \\ \mathbf{B}_n^{N0} & \mathbf{B}_n^{N1} & \ldots & \mathbf{B}_n^{NN} \end{bmatrix} \end{aligned} \tag{36}$$

are square matrices of dimension $3(N + 1)$, and

$$\mathbf{u}_m(x) = \begin{bmatrix} \mathbf{u}_{0m}^{\mathrm{T}}(x) & \mathbf{u}_{1m}^{\mathrm{T}}(x) & \ldots & \mathbf{u}_{Nm}^{\mathrm{T}}(x) \end{bmatrix}^{\mathrm{T}} \tag{37}$$

A state space approach is employed to solve the free vibration problem by converting Eqs. (35) into a

first-order representation as follows

$$\begin{cases} \dfrac{\mathrm{d}\mathbf{z}_m}{\mathrm{d}x} = \mathbf{A}\mathbf{z}_m \\ \mathbf{B}\mathbf{z}_m(0) = \mathbf{0} \\ \mathbf{B}\mathbf{z}_m(a) = \mathbf{0} \end{cases} \tag{38}$$

where

$$\mathbf{z}_m(x) = \begin{Bmatrix} \mathrm{d}\mathbf{u}_m/\mathrm{d}x \\ \mathbf{u}_m \end{Bmatrix} \tag{39}$$

and

$$\mathbf{A} = \begin{bmatrix} \mathbf{L}_2 & \mathbf{0} \\ \mathbf{0} & \mathbf{I} \end{bmatrix}^{-1} \begin{bmatrix} \mathbf{L}_1 & \mathbf{L}_0 \\ \mathbf{I} & \mathbf{0} \end{bmatrix}, \qquad \mathbf{B} = \begin{bmatrix} \mathbf{B}_1 & \mathbf{B}_0 \end{bmatrix} \tag{40}$$

The general solution of Eq. (38) can be expressed as

$$\mathbf{z}_m(x) = e^{\mathbf{A}x}\mathbf{c}_m \tag{41}$$

where $\mathbf{c}_m$ is a vector of constants to be determined from boundary conditions. Using a spectral decomposition of the exponential matrix, the solution can be written as

$$\mathbf{z}_m(x) = \mathbf{V}\mathrm{Diag}\left(e^{\lambda_i x}\right)\mathbf{V}^{-1}\mathbf{c}_m \tag{42}$$

where $\mathbf{V}$ is the matrix of eigenvectors of $\mathbf{A}$ and λ_i are the corresponding eigenvalues. Replacement of solution (42) into the system of boundary equations in Eq. (38) yields a homogeneous system

$$\mathbf{H}\mathbf{c}_m = \mathbf{0} \qquad (x = 0, a) \tag{43}$$

where

$$\mathbf{H} = \mathbf{B}\mathbf{V}\mathrm{Diag}\left(e^{\lambda_i x}\right)\mathbf{V}^{-1} \tag{44}$$

The natural frequencies associated with the m-th mode are determined by setting the determinant of $\mathbf{H}$ equal to zero. Since $\mathbf{H} = \mathbf{H}(\omega_m)$, an iterative numerical procedure is employed to derive the frequency parameters.

4. Modal displacement and stress distributions

Once the frequency values are computed, modal displacement and stress distributions at any point (ξ, η, ζ) of the plate can be recovered. The procedure for the m-th mode involves the following steps:

1. Matrix $\mathbf{A}$ in Eq. (40) is evaluated at the natural frequency ω_m.
2. Matrix $\mathbf{H}$ is computed from Eq. (44) at coordinate ξ.
3. The homogeneous system in Eq. (43) is solved for the non-trivial vector of coefficients $\mathbf{c}_m$ and the corresponding state vector $\mathbf{z}_m(\xi)$ is computed using Eq. (42).

4. The vector $\mathbf{u}_m(\xi)$ containing the amplitudes $\mathbf{u}_{\tau m}(\xi)$ is extracted form the state vector and the modal displacements are recovered from Eqs. (4) and (24) as

$$\begin{aligned} u(\xi,\eta,\zeta) &= F_\tau(\zeta) u_{\tau m}(\xi)\sin(\beta_m \eta) \\ v(\xi,\eta,\zeta) &= F_\tau(\zeta) v_{\tau m}(\xi)\cos(\beta_m \eta) \\ w(\xi,\eta,\zeta) &= F_\tau(\zeta) w_{\tau m}(\xi)\sin(\beta_m \eta) \end{aligned} \tag{45}$$

5. The vector $\mathrm{d}\mathbf{u}_m(\xi)/\mathrm{d}x$ containing the amplitudes $\mathrm{d}\mathbf{u}_{\tau m}(\xi)/\mathrm{d}x$ is extracted form the state vector and the modal in-plane stress components are derived by substituting the strain-displacement relations (3) into the constitutive equations (14). This yields

$$\begin{aligned} \sigma_{xx}(\xi,\eta,\zeta) &= \Bigg[C_{11}(\zeta) F_\tau(\zeta) \frac{\mathrm{d}u_{\tau m}}{\mathrm{d}x}(\xi) \\ &\quad - \beta_m C_{12}(\zeta) F_\tau(\zeta) v_{\tau m}(\xi) + C_{13}(\zeta) \frac{\mathrm{d}F_\tau}{\mathrm{d}z}(\zeta) w_{\tau m}(\xi) \Bigg] \sin(\beta_m \eta) \\ \sigma_{xy}(\xi,\eta,\zeta) &= C_{66}(\zeta) F_\tau(\zeta) \left[\frac{\mathrm{d}v_{\tau m}}{\mathrm{d}x}(\xi) + \beta_m u_{\tau m}(\xi) \right] \cos(\beta_m \eta) \\ \sigma_{yy}(\xi,\eta,\zeta) &= \Bigg[C_{12}(\zeta) F_\tau(\zeta) \frac{\mathrm{d}u_{\tau m}}{\mathrm{d}x}(\xi) \\ &\quad - \beta_m C_{22}(\zeta) F_\tau(\zeta) v_{\tau m}(\xi) + C_{23}(\zeta) \frac{\mathrm{d}F_\tau}{\mathrm{d}z}(\zeta) w_{\tau m}(\xi) \Bigg] \sin(\beta_m \eta) \end{aligned} \tag{46}$$

6. The modal transverse shear and normal stresses are evaluated by integrating the 3-D equations of motion of the FGM plate in the thickness direction so that the stress boundary conditions on the top and bottom surfaces can be satisfied. The 3-D equilibrium of the plate may be written in the following form

$$\begin{aligned} \sigma_{xz} &= \int_{-h/2}^{z} \left[\rho \ddot{u} - \frac{\partial \sigma_{xx}}{\partial x} - \frac{\partial \sigma_{xy}}{\partial y} \right] \mathrm{d}z + C_x \\ \sigma_{yz} &= \int_{-h/2}^{z} \left[\rho \ddot{v} - \frac{\partial \sigma_{xy}}{\partial x} - \frac{\partial \sigma_{yy}}{\partial y} \right] \mathrm{d}z + C_y \\ \sigma_{zz} &= \int_{-h/2}^{z} \left[\rho \ddot{w} - \frac{\partial \sigma_{xz}}{\partial x} - \frac{\partial \sigma_{yz}}{\partial y} \right] \mathrm{d}z + C_z \end{aligned} \tag{47}$$

where C_x, C_y and C_z are integration constants. After computing $\mathrm{d}\mathbf{z}_m(\xi)/\mathrm{d}x$ from Eq. (38) and imposing null conditions of transverse stresses at plate top and bottom, the modal stresses are given

by

$$
\begin{aligned}
\sigma_{xz}(\xi,\eta,\zeta) &= \Big[-\omega_m^2\mathcal{I}_{\rho\tau}(\zeta)u_{\tau m}(\xi) - \mathcal{I}^0_{11\tau}(\zeta)\frac{\mathrm{d}^2u_{\tau m}}{\mathrm{d}x^2}(\xi) \\
&+ \beta_m\mathcal{I}^0_{12\tau}(\zeta)\frac{\mathrm{d}v_{\tau m}}{\mathrm{d}x}(\xi) - \mathcal{I}^1_{13\tau}(\zeta)\frac{\mathrm{d}w_{\tau m}}{\mathrm{d}x}(\xi) \\
&+ \beta_m\mathcal{I}^0_{66\tau}(\zeta)\frac{\mathrm{d}v_{\tau m}}{\mathrm{d}x}(\xi) + \beta_m^2\mathcal{I}^0_{66\tau}(\zeta)u_{\tau m}(\xi)\Big]\sin(\beta_m\eta) \\
\sigma_{yz}(\xi,\eta,\zeta) &= \Big[-\omega_m^2\mathcal{I}_{\rho\tau}(\zeta)v_{\tau m}(\xi) - \beta_m\mathcal{I}^0_{12\tau}(\zeta)\frac{\mathrm{d}u_{\tau m}}{\mathrm{d}x}(\xi) \\
&+ \beta_m^2\mathcal{I}^0_{22\tau}(\zeta)v_{\tau m}(\xi) - \beta_m\mathcal{I}^1_{23\tau}(\zeta)w_{\tau m}(\xi) \\
&+ \mathcal{I}^0_{66\tau}(\zeta)\frac{\mathrm{d}^2v_{\tau m}}{\mathrm{d}x^2}(\xi) + \beta_m\mathcal{I}^0_{66\tau}(\zeta)\frac{\mathrm{d}u_{\tau m}(\xi)}{\mathrm{d}x}\Big]\cos(\beta_m\eta) \\
\sigma_{zz}(\xi,\eta,\zeta) &= \Big[-\omega_m^2\mathcal{I}_{\rho\tau}(\zeta)w_{\tau m}(\xi) - \mathcal{I}^0_{55\tau}(\zeta)\frac{\mathrm{d}^2w_{\tau m}}{\mathrm{d}x^2}(\xi) \\
&- \mathcal{I}^1_{55\tau}(\zeta)\frac{\mathrm{d}u_{\tau m}}{\mathrm{d}x}(\xi) + \beta_m^2\mathcal{I}^0_{44\tau}(\zeta)w_{\tau m}(\xi) \\
&+ \beta_m\mathcal{I}^1_{44\tau}(\zeta)v_{\tau m}(\xi)\Big]\sin(\beta_m\eta)
\end{aligned}
\tag{48}
$$

where

$$
\mathcal{I}_{\rho\tau}(\zeta) = \int_{-h/2}^{\zeta}\rho(z)F_\tau(z)\mathrm{d}z \tag{49}
$$

and

$$
\mathcal{I}^\alpha_{ij\tau}(\zeta) = \int_{-h/2}^{\zeta}C_{ij}(z)\frac{\mathrm{d}^\alpha F_\tau}{\mathrm{d}z^\alpha}(z)\mathrm{d}z \tag{50}
$$

5. Effective material properties

Many methods are available to estimate the effective properties of functionally graded materials fabricated by mixing two discrete phases of materials. Due to inaccurate knowledge of particles geometry and distribution, they are often based only on the volume fraction distribution of the dispersed phase [4]. Assuming a two-constituents FGM plate involving mixture of a metal and a ceramic, the volume fraction of the ceramic phase is here assumed to be given by the following power-law function

$$
V_c(z) = V_c^{\mathrm{bot}} + \left(V_c^{\mathrm{top}} - V_c^{\mathrm{bot}}\right)\left(\frac{1}{2} + \frac{z}{h}\right)^p \tag{51}
$$

where V_c^{bot} and V_c^{top} are the volume fractions of the ceramic phase on the bottom and top surfaces of the plate, respectively, and p is the parameter describing the profile across the thickness. The volume fraction of the metal phase is given by

$$
V_m(z) = 1 - V_c(z) \tag{52}
$$

Therefore, the effective mass density of the FGM plate is obtained as

$$\rho(z) = \rho_m V_m(z) + \rho_c V_c(z) \tag{53}$$

where ρ_m and ρ_c are the mass densities of the metal and ceramic phase, respectively.

The effective elastic moduli are estimated in this work according to two common procedures, the rule-of-mixtures and the Mori-Tanaka scheme. It is worth noting that the mathematical formulation presented in previous sections is completely general and other homogenization procedures can be adopted. According to the rule-of-mixtures, the effective Young's modulus and Poisson's ratio are expressed in the same way as the mass density. It follows that

$$E(z) = E_m V_m(z) + E_c V_c(z) \tag{54}$$

$$\nu(z) = \nu_m V_m(z) + \nu_c V_c(z) \tag{55}$$

The above relations are very simple but they can be very approximate [13]. A slightly more complicated scheme which yields more accurate estimates of the effective elastic moduli is the Mori-Tanaka homogenization procedure [2]. First, it involves the computation of the effective bulk modulus K and shear modulus G starting from the bulk and shear moduli of the metal and ceramic phase as follows

$$K(z) = K_m + \frac{V_c(z)\,(K_c - K_m)}{1 + V_m(z)\frac{K_c - K_m}{K_m + k_m}} \tag{56}$$

$$G(z) = G_m + \frac{V_c(z)\,(G_c - G_m)}{1 + V_m(z)\frac{G_c - G_m}{G_m + g_m}} \tag{57}$$

where

$$k_m = \frac{4}{3} G_m \qquad\qquad g_m = \frac{G_m\,(9K_m + 8G_m)}{6\,(K_m + 2G_m)} \tag{58}$$

Then, the effective elastic moduli at any point z along the thickness of the FGM plate are determined using the following relations

$$E(z) = \frac{9K(z)G(z)}{3K(z) + G(z)} \tag{59}$$

$$\nu(z) = \frac{1}{2}\frac{3K(z) - 2G(z)}{3K(z) + G(z)} \tag{60}$$

6. Numerical analysis

Some free vibration results are presented in this section according to the proposed exact formulation. The numerical analysis is carried out using a family of HOSNTs where the in-plane and out-of-plane displacements of the plate are expanded as Taylor's series of the thickness coordinates, i.e.,

$$F_\tau(z) = z^\tau \tag{61}$$

In particular, three theories of different order N are evaluated. For the sake of brevity, they are denoted as HOSNT-n, where n is the number of kinematic variables included in the plate model. The three theories correspond to $N = 2, 3$ and 4 in Eq. (4) and are written explicitly in the following:

$$\text{HOSNT-9:} \quad \begin{cases} u = u_0 + zu_1 + z^2u_2 \\ v = v_0 + zv_1 + z^2v_2 \\ w = w_0 + zw_1 + z^2w_2 \end{cases} \tag{62}$$

$$\text{HOSNT-12:} \quad \begin{cases} u = u_0 + zu_1 + z^2u_2 + z^3u_3 \\ v = v_0 + zv_1 + z^2v_2 + z^3v_3 \\ w = w_0 + zw_1 + z^2w_2 + z^3w_3 \end{cases} \tag{63}$$

$$\text{HOSNT-15:} \quad \begin{cases} u = u_0 + zu_1 + z^2u_2 + z^3u_3 + z^4u_4 \\ v = v_0 + zv_1 + z^2v_2 + z^3v_3 + z^4v_4 \\ w = w_0 + zw_1 + z^2w_2 + z^3w_3 + z^4w_4 \end{cases} \tag{64}$$

It is noted that the first-order theory HOSNT-6 is not considered since a constant distribution of transverse normal strain arising from the linear expansion of the transverse displacement introduces a severe thickness locking problem [14], especially for thin and moderately thick plates. As explained in Ref. [14], in order to avoid locking, HOSNT-6 can be used with the condition of null transverse normal stresses. In this way, HOSNT-6 is actually reduced to FOST.

The mathematical formulation here presented is first compared with exact 3-D natural frequencies obtained by Vel and Batra [4] for a square simply-supported Al/ZrO_2 plate of various length-to-thickness ratio a/h and different power-law exponents p. Constituent materials of the FGM plate have the following properties:

$$\text{Al}: \qquad E_m = 70 \text{ GPa}, \quad \nu_m = 0.3, \quad \rho_m = 2702 \text{ kg/m}^3$$

$$\text{ZrO}_2: \qquad E_c = 200 \text{ GPa}, \quad \nu_c = 0.3, \quad \rho_c = 5700 \text{ kg/m}^3$$

Table 1 shows the dimensionless fundamental frequency $\lambda = \omega h\sqrt{\rho_m/E_m}$ for moderately thick ($a/h =$ 20 and 10) and thick ($a/h = 5$) plates with $p = 1$ and for thick plates with $a/h = 5$ and $p = 2, 3, 5$. Elastic properties of the graded plate are computed using the Mori-Tanaka homogenization scheme as in Ref. [4]. Present exact results are also compared with analytical solutions in Ref. [8] obtained using FOST and with numerical values provided by Neves et al. [15] and Qian and Batra [13] using different HOSNTs. In particular, results in Ref. [15] are computed with the radial basis functions collocation technique and analysis in Ref. [13] is performed with the meshless local Petrov-Galerkin method. It is also noted that in Ref. [8] the material properties of the FGM plate are estimated by the rule-of-mixtures. From Table 1 it can be observed that all present exact solutions are in excellent agreement with 3-D analysis for moderately thick plates. When the length-to-thickness ratio decreases, the error of the plate model

HOSNT-9 increases and theories of higher order are required to achieve highly accurate results. Note also that, for $a/h = 5$, the discrepancy between HOSNT-9 and 3-D elasticity solutions increases with increasing power-law exponent p. However, the error remains acceptable with a difference below 2% for the cases under investigation. To further validate the present formulation, Figure 1a and 1b show the through-the-thickness modal distribution of the normalized in-plane stress $\sigma_{xx}(a/2, b/2)/\max|\sigma_{xx}(a/2, b/2)|$ and transverse normal stress $\sigma_{zz}(a/2, b/2)/\max|\sigma_{zz}(a/2, b/2)|$, respectively, when $a/h = 5$ and $p = 3$. The exact modal stress profile reported in Ref. [4] is compared with that estimated from Eqs. (46) and (48) using HOSNT-15. It is clearly seen that they agree well. The unsymmetric and non-linear distribution of the in-plane stress arising from the variation of the material properties along the thickness direction is also pointed out.

Another numerical validation of the present approach is provided in Table 2 for the same plate considered before. The attention is now focused on the estimation of the natural frequency of the first three thickness modes. Present results are tabulated only for HOSNT-15. It is shown that the assumed fourth-order 2-D plate model is capable of providing a very good correlation with elasticity solution in all cases. From this and the previous analysis, it can be argued that HOSNT-15 exhibits an accuracy comparable to 3-D formulation. Therefore, the corresponding solutions will be taken as accurate references in the studies presented below.

Table 3 shows the first ten natural frequencies of the square Al/ZrO_2 simply-supported plate with $p = 1$ and various length-to-thickness ratios. Dimensionless values $\lambda = \omega h\sqrt{\rho_m/E_m}$ are computed using HOSNT-9, HOSNT-12 and HOSNT-15. To the best author's knowledge, no exact 3-D results or other analytical 2-D solutions are available for this particular case. Therefore, the values computed by 2-D meshless methods in Refs. [13] and [15] are used as reference for checking the correctness of the proposed formulation. At the same time, the accuracy of the above numerical approaches can be evaluated by comparison with the present exact analysis. From Table 3 it is observed that HOSNT-12 and HOSNT-15 give the same values for all modes when the plate is moderately thick ($a/h = 20$ and 10). For plates with $a/h = 5$, frequencies computed by HOSNT-12 and related to predominantly flexural modes are slightly higher than those of HOSNT-15 and the difference increases for modes at higher frequencies. By comparison with HOSNT-15, it is shown that HOSNT-9 is accurate when $a/h = 20$ and acceptable for plates with $a/h = 10$. Therefore, including higher-order terms in the kinematic model has no significant contribution for those cases. However, when the plate gets thicker, the difference becomes considerable, especially if higher frequencies are of interest. For example, the discrepancy between HOSNT-9 and HOSNT-15 is 1.8% for the fourth mode and increases to about 3% for mode 10. Table 3 also shows that the numerical method developed by Neves et al. [15] is highly accurate. On the contrary, values provided by Qian and Batra [13] are generally underestimated with respect to HOSNT-15. This may be due to the fact that, as stated by the authors, the Poisson's ratio has been taken as 0.3 throughout the plate, instead of the value given by Eq. (60) according to the Mori-Tanaka procedure.

After extensive validation of the present formulation for simply-supported plates, free vibration anal-

ysis of moderately thick and thick Lévy FGM plates is now discussed. Six different combinations of clamped (C), free (F) and simply-supported (S) conditions at $x = 0, a$ are considered in the following: simply-supported/simply-supported, simply-supported/clamped, clamped/clamped, free/free, free/simply-supported and free/clamped. Each combination will be shortly indicated by a two-letter notation corresponding to edge conditions at $x = 0$ and $x = a$. For example, FC stands for a Lévy plate with free edge at $x = 0$ and clamped edge at $x = a$.

First, a comparison with the analytical study of Hosseini-Hashemi [8] is performed for SC and CC square Al/Al_2O_3 plates with $a/h = 20$ and $a/h = 5$. The elastic properties of Alumina are assumed to be the following:

$$Al_2O_3: \qquad E_c = 380 \text{ GPa}, \quad \nu_c = 0.3, \quad \rho_c = 3800 \text{ kg/m}^3$$

Elastic properties of the graded plate are here computed according to the rule-of-mixtures as in Ref. [8]. Table 4 reports the first two frequency parameters $\lambda = \omega a^2 \sqrt{\rho_c / E_c}$ corresponding to $m = 1$ and $m = 2$, for different values of power-law exponent p. For the sake of brevity, only results computed on the basis of HOSNT-15 are tabulated. It is shown that, for both SC and CC plates, FOST generally underestimates frequency parameters when $p = 1$ and $p = 2$, whereas values higher than those of HOSNT-15 are obtained for larger p. Such inconsistency may be due to the value of the shear correction factor, which is arbitrarily taken as 5/6 [8]. Note also that the over-correction of FOST for $p = 1, 2$ is more pronounced in thick plates.

The next two examples aim at presenting new results of Lévy FGM plates, which can be also useful as benchmarks for future numerical studies.

Figures 2 and 3 display non-dimensionalized modal stresses $\overline{\sigma}_{xx}$ and $\overline{\sigma}_{zz}$ versus the power-law index p corresponding to the fundamental mode of a Al/ZrO_2 square plate with $a/h = 5$. The whole set of boundary conditions described above is encompassed. The longitudinal and transverse normal stress values are computed as follows

$$\overline{\sigma}_{xx} = \frac{\sigma_{xx}(a/2, b/2, h/2)a^2}{10 E_m w(a/2, b/2, 0)h} \tag{65}$$

$$\overline{\sigma}_{zz} = \frac{\sigma_{zz}(a/2, b/2, 0)a^4}{E_m w(a/2, b/2, 0)h^3} \tag{66}$$

Through-the-thickness variation of the elastic moduli are estimated according to the Mori-Tanaka scheme and the stress distributions are obtained using HOSNT-15. It is seen that the largest effect of different boundary conditions is to shift the minimum value attained by $\overline{\sigma}_{xx}$ as p increases from 1 to 5. In particular, Fig. 2 shows that the minimum value of $\overline{\sigma}_{xx}$ occurs at $p \approx 2$ for SS plates and moves to $p \approx 2.4$ and $p \approx 3$ for SC and CC plates, respectively. On the contrary, the maximum of $\overline{\sigma}_{zz}$ is rather insensitive to changes in the boundary conditions and occurs for p slightly greater than 2.

The last analysis deals with the numerical case considered by Vel and Batra [4] and selected as first validation case at the beginning of this section. However, the exact vibration analysis is here extended

to different plate boundaries and performed using 2-D theories. Table 5 shows the non-dimensionalized fundamental frequency of Al/ZrO_2 plates with $a/h = 20, 10, 5$ and $p = 1, 2, 3, 5$ for each combination of edge conditions. As a result, a comprehensive set of results is generated. The observations made before on fully simply-supported plates are also valid when different boundary conditions are considered. HOSNT-9 is to be preferred for moderately thick plates since it provides comparable accuracy to theories of higher order with less number of kinematic variables. For thick plates having $a/h = 5$, HOSNT-12 and HOSNT-15 are in general significantly more accurate, especially when clamped edges are involved.

7. Conclusions

Exact free vibration analysis of moderately thick and thick Lévy FGM plates using two-dimensional higher-order kinematic theories with both shear and normal deformation effects is presented. The formulation relies on a powerful indicial notation and the state-space approach so that the burden of deriving the governing equations and the corresponding solution each time a different plate model is assumed is highly reduced. In this way, new exact frequency results computed on the basis of kinematic theories of different orders can be easily obtained in a somehow automatic manner.

The numerical analysis is carried out in this work using a specific family of higher-order shear and normal deformation theories and the elastic properties of the graded plate are estimated by the Mori-Tanaka procedure or the rule-of-mixtures. Anyway, the mathematical formulation is written in general terms and can be directly applied to other plate models and material homogenization schemes.

The present approach is first validated on fully simply-supported FGM plates by comparison with exact 3-D solutions and other 2-D frequency results. Then, some examples of FGM plates with at least two opposite edges simply-supported are provided for the first time. It is shown that theories of high order are highly recommended in the following cases:

1. the length-to-thickness ratio a/h of the FGM plate is below 10;
2. frequency modes higher than the fundamental one are to be estimated with accuracy;
3. the FGM plate is characterized by a large value of the power-law exponent describing the variation of elastic properties through the thickness;
4. the FGM plate involves one or two clamped edges.

By comparison with some exact solutions available in the literature, it is also noted that the first-order shear deformation theory underestimates the frequency values in many cases. Such effect, which is probably due to the value of the shear correction factor, is strongly dependent on the boundary conditions, the power-law exponent and the length-to-thickness ratio of the FGM plate.

A rather comprehensive set of exact frequency results corresponding to the fundamental frequency of various square FGM plates with six combinations of boundary conditions is provided. The tabulated values may serve as valuable sources for validating other approaches and approximate methods.

References

[1] D.K. Jha, Tarun Kant, R.K. Singh, A critical review of recent research on functionally graded plates, *Composite Structures*, 96 (2013), 833-849.

[2] T. Mori, K. Tanaka, Average stress in matrix and average elastic energy of materials with misfitting inclusions, *Acta Metallurgica*, 21 (1973), 571-574.

[3] A.W. Leissa, The free vibration of rectangular plates, *Journal of Sound and Vibration*, 31 (1973), 257-293.

[4] S.S. Vel, R.C. Batra, Three-dimensional exact solution for the vibration of functionally graded rectangular plates, *Journal of Sound and Vibration*, 272 (2004), 703-730.

[5] H. Matsunaga, Free vibration and stability of functionally graded plates according to a 2-D higher-order deformation theory, *Composite Structures*, 82 (2008), 499-512.

[6] D.K. Jha, Tarun Kant, R.K. Singh, Free vibration response of functionally graded thick plates with shear and normal deformation effects, *Composite Structures*, 96 (2013), 799-823.

[7] A. Hasani Baferani, A.R. Saidi, E. Jomehzadeh, An exact solution for free vibration of thin functionally graded rectangular plates, *Proceedings of the Institution of Mechanical Engineers, Part C: Journal of Mechanical Engineering Science*, 225 (2011), 526-536.

[8] Sh. Hosseini-Hashemi, M. Fadaee, S.R. Atashipour, A new exact analytical approach for free vibration of Reissner-Mindlin functionally graded rectangular plates, *International Journal of Mechanical Sciences*, 53 (2011), 11-22.

[9] Sh. Hosseini-Hashemi, M. Fadaee, S.R. Atashipour, Study on the free vibration of thick functionally graded rectangular plates according to a new exact closed-form procedure, *Composite Structures*, 93 (2011), 722-735.

[10] J.N. Reddy, A simple higher-order theory for laminated composite plates, *Journal of Applied Mechanics*, 51 (1984), 745-752.

[11] A. Hasani Baferani, A.R. Saidi, H. Ehteshami, Accurate solution for free vibration analysis of functionally graded thick rectangular plates resting on elastic foundation, *Composite Structures*, 93 (2011), 1842-1853.

[12] L. Dozio, Exact vibration solutions for cross-ply laminated plates with two opposite edges simply supported using refined theories of variable order, *Journal of Sound and Vibration*, accepted, in press.

[13] L.F. Qian, R.C. Batra, L.M. Chen, Static and dynamic deformations of thick functionally graded elastic plates by using higher-order shear and normal deformable plate theory and meshless local Petrov-Galerkin method, *Composites: Part B*, 35 (2004), 685-697.

[14] E. Carrera, S. Brischetto, Analysis of thickness locking in classical, refined and mixed multilayered plate theories, *Composite Structures*, 82 (2008), 549-562.

[15] A.M.A. Neves, A.J.M. Ferreira, E. Carrera, M. Cinefra, C.M.C. Roque, R.M.N. Jorge, C.M.M. Soares, Static, free vibration and buckling analysis of isotropic and sandwich functionally graded plates using a quasi-3D higher-order shear deformation theory and a meshless technique, *Composites: Part B*, 44 (2013), 657-674.

Table 1: Comparison of fundamental frequency $\lambda = \omega h\sqrt{\rho_m/E_m}$ for square simply-supported Al/ZrO_2 plates.

	$p=1$			$a/h=5$		
Model	$a/h=20$	$a/h=10$	$a/h=5$	$p=2$	$p=3$	$p=5$
Exact 3D [4]	0.0153	0.0596	0.2192	0.2197	0.2211	0.2225
HOSNT-15	0.0154	0.0596	0.2191	0.2196	0.2211	0.2225
HOSNT-12	0.0154	0.0596	0.2193	0.2198	0.2211	0.2226
HOSNT-9	0.0154	0.0597	0.2213	0.2225	0.2245	0.2263
Ref. [15]	0.0153	0.0596	0.2193	0.2200	0.2215	0.2230
Ref. [13]	0.0149	0.0584	0.2152	0.2153	0.2172	0.2194
Ref. [8]	0.0158	0.0619	0.2276	0.2264	0.2276	0.2291

Table 2: Comparison of thickness mode frequencies $\lambda = \omega h\sqrt{\rho_m/E_m}$ for square simply-supported Al/ZrO_2 plates.

		$p=1$			$a/h=5$		
Thickness mode	Model	$a/h=20$	$a/h=10$	$a/h=5$	$p=2$	$p=3$	$p=5$
2	Exact 3D [4]	0.1456	0.2912	0.5823	0.5711	0.5660	0.5610
	HOSNT-15	0.1456	0.2911	0.5820	0.5709	0.5659	0.5610
3	Exact 3D [4]	0.2454	0.4901	0.9752	0.9564	0.9478	0.9398
	HOSNT-15	0.2452	0.4899	0.9748	0.9560	0.9476	0.9396
4	Exact 3D [4]	2.0598	2.0750	2.1346	2.0150	1.9530	1.9075
	HOSNT-15	2.0594	2.0745	2.1341	2.0159	1.9548	1.9095

Figure 1: The fundamental through-the-thickness stress mode shape for a Al/ZrO_2 simply-supported square plate with $p = 3$ and $a/h = 5$. (a) Normalized in-plane stress $\sigma_{xx}(a/2, b/2)/\max|\sigma_{xx}(a/2, b/2)|$. (b) Normalized transverse normal stress $\sigma_{zz}(a/2, b/2)/\max|\sigma_{zz}(a/2, b/2)|$. Legend: –, present analysis with HOSNT-15; ∘, exact 3D values from Ref. [4].

Figure 2: Non-dimensional stress $\overline{\sigma}_{xx}$ (a) and $\overline{\sigma}_{zz}$ (b) versus p corresponding to the fundamental mode of a Al/ZrO_2 square plate with $a/h = 5$ and various boundary conditions. Legend: —— SS; –. SC; –– CC.

Figure 3: Non-dimensional stress $\overline{\sigma}_{xx}$ (a) and $\overline{\sigma}_{zz}$ (b) versus p corresponding to the fundamental mode of a Al/ZrO_2 square plate with $a/h = 5$ and various boundary conditions. Legend: —— FF; –. FS; –– FC.

Table 3: First 10 natural frequencies $\lambda = \omega h\sqrt{\rho_m/E_m}$ of square simply-supported Al/ZrO_2 plates with $p = 1$ and various thickness ratios.

		Mode									
a/h	Model	1	2	3	4	5	6	7	8	9	10
20	HOSNT-15	0.0154	0.0377	0.0377	0.0596	0.0740	0.0740	0.0950	0.0950	0.1030	0.1030
	HOSNT-12	0.0154	0.0377	0.0377	0.0596	0.0740	0.0740	0.0950	0.0950	0.1030	0.1030
	HOSNT-9	0.0154	0.0379	0.0379	0.0597	0.0742	0.0742	0.0955	0.0955	0.1030	0.1030
	Ref. [13]	0.0149	0.0377	0.0377	0.0593	0.0747	0.0747	0.0769	0.0912	0.0913	0.1029
	Ref. [15]	0.0153	0.0377	0.0377	0.0596	0.0739	0.0739	0.0950	0.0950	0.1030	0.1030
10	HOSNT-15	0.0596	0.1425	0.1425	0.2059	0.2059	0.2191	0.2674	0.2674	0.2911	0.3359
	HOSNT-12	0.0596	0.1425	0.1425	0.2059	0.2059	0.2193	0.2674	0.2674	0.2911	0.3360
	HOSNT-9	0.0597	0.1435	0.1435	0.2059	0.2059	0.2213	0.2704	0.2704	0.2911	0.3405
	Ref. [13]	0.0584	0.1410	0.1410	0.2058	0.2058	0.2164	0.2646	0.2677	0.2913	0.3264
	Ref. [15]	0.0596	0.1426	0.1426	0.2059	0.2059	0.2193	0.2676	0.2676	0.2912	0.3364
5	HOSNT-15	0.2191	0.4116	0.4116	0.4820	0.4820	0.5820	0.6996	0.8228	0.8281	0.8281
	HOSNT-12	0.2193	0.4116	0.4116	0.4824	0.4824	0.5820	0.7004	0.8228	0.8293	0.8293
	HOSNT-9	0.2213	0.4116	0.4116	0.4906	0.4906	0.5820	0.7159	0.8229	0.8496	0.8496
	Ref. [13]	0.2152	0.4114	0.4114	0.4761	0.4761	0.5820	0.6914	0.8192	0.8217	0.8242

Table 4: First two natural frequencies $\lambda = \omega a^2\sqrt{\rho_c/E_c}$ corresponding to $m = 1$ and $m = 2$ of square Al/Al_2O_3 plates with different boundary conditions and thickness ratios. Elastic properties of the graded plate are computed according to the rule-of-mixtures.

Boundary					Power law index (p)				
conditions	a/h	m	Mode	Model	1	2	5	8	10
SC	20	1	1	HOSNT-15	5.4207	4.9117	4.6318	4.5554	4.4791
				FOST [8]	5.3926	4.9019	4.6382	4.5443	4.4854
			2	HOSNT-15	13.208	11.987	11.249	11.020	10.867
				FOST [8]	13.159	11.956	11.283	11.040	10.893
		2	1	HOSNT-15	11.707	10.612	10.002	9.7980	9.6707
				FOST [8]	11.667	10.601	10.016	9.8068	9.6779
			2	HOSNT-15	19.189	17.407	16.313	15.931	15.728
				FOST [8]	19.136	17.380	16.379	16.016	15.800
	5	1	1	HOSNT-15	4.6763	4.2055	3.8285	3.7061	3.6504
				FOST [8]	4.6356	4.1996	3.8916	3.7746	3.7146
			2	HOSNT-15	9.5960	8.6448	7.4598	6.9970	6.8172
				FOST [8]	9.8739	8.9239	8.1442	7.8438	7.7031
		2	1	HOSNT-15	9.3272	8.3553	7.4948	7.2181	7.1067
				FOST [8]	9.2165	8.3310	7.6567	7.4012	7.2768
			2	HOSNT-15	13.805	12.322	10.867	10.398	10.223
				FOST [8]	13.571	12.249	11.142	10.717	10.521
CC	20	1	1	HOSNT-15	6.5914	5.9806	5.6243	5.5225	5.4462
				FOST [8]	6.5585	5.9612	5.6332	5.5152	5.4423
			2	HOSNT-15	15.448	13.997	13.106	12.801	12.648
				FOST [8]	15.390	13.981	13.167	12.869	12.693
		2	1	HOSNT-15	12.343	11.198	10.536	10.307	10.180
				FOST [8]	12.305	11.181	10.555	10.330	10.193
			2	HOSNT-15	20.894	18.934	17.687	17.280	17.051
				FOST [8]	20.816	18.904	17.785	17.376	17.136
	5	1	1	HOSNT-15	5.3714	4.8147	4.3216	4.1626	4.0973
				FOST [8]	5.3039	4.8032	4.4127	4.2604	4.1865
			2	HOSNT-15	10.915	9.7296	8.5287	8.1454	8.0038
				FOST [8]	10.712	9.6759	8.7548	8.3957	8.2345
		2	1	HOSNT-15	9.5833	8.5764	7.6618	7.3676	7.2515
				FOST [8]	9.4561	8.5466	7.8331	7.5610	7.4307
			2	HOSNT-15	14.314	12.763	11.188	10.679	10.495
				FOST [8]	14.040	12.670	11.473	11.011	10.802

Table 5: Exact dimensionless fundamental frequency $\lambda = \omega h\sqrt{\rho_m/E_m}$ of square Al/ZrO_2 plate with various side-to-thickness ratios a/h, power-law exponents p and different combinations of boundary conditions along x direction. Elastic properties of the graded plate are computed using the Mori-Tanaka homogenization scheme.

			Boundary conditions					
a/h	p	Model	SS	SC	CC	FF	FS	FC
20	1	HOSNT-9	0.0154	0.0183	0.0222	0.0075	0.0091	0.0099
		HOSNT-12	0.0154	0.0183	0.0222	0.0075	0.0091	0.0099
		HOSNT-15	0.0154	0.0183	0.0222	0.0075	0.0091	0.0099
	2	HOSNT-9	0.0155	0.0185	0.0225	0.0076	0.0093	0.0100
		HOSNT-12	0.0155	0.0185	0.0224	0.0076	0.0093	0.0100
		HOSNT-15	0.0155	0.0185	0.0224	0.0076	0.0093	0.0100
	3	HOSNT-9	0.0158	0.0188	0.0227	0.0077	0.0094	0.0101
		HOSNT-12	0.0156	0.0186	0.0226	0.0077	0.0094	0.0101
		HOSNT-15	0.0156	0.0186	0.0226	0.0077	0.0094	0.0101
	5	HOSNT-9	0.0159	0.0189	0.0230	0.0077	0.0094	0.0102
		HOSNT-12	0.0159	0.0189	0.0229	0.0077	0.0094	0.0101
		HOSNT-15	0.0159	0.0189	0.0229	0.0077	0.0094	0.0101
10	1	HOSNT-9	0.0597	0.0705	0.0845	0.0296	0.0356	0.0385
		HOSNT-12	0.0596	0.0703	0.0839	0.0295	0.0356	0.0384
		HOSNT-15	0.0596	0.0701	0.0839	0.0295	0.0356	0.0384
	2	HOSNT-9	0.0604	0.0711	0.0851	0.0299	0.0360	0.0389
		HOSNT-12	0.0601	0.0708	0.0843	0.0299	0.0359	0.0387
		HOSNT-15	0.0601	0.0706	0.0843	0.0299	0.0359	0.0387
	3	HOSNT-9	0.0611	0.0720	0.0860	0.0302	0.0365	0.0394
		HOSNT-12	0.0607	0.0714	0.0850	0.0301	0.0364	0.0391
		HOSNT-15	0.0607	0.0714	0.0849	0.0301	0.0364	0.0391
	5	HOSNT-9	0.0617	0.0726	0.0868	0.0306	0.0369	0.0398
		HOSNT-12	0.0614	0.0720	0.0855	0.0305	0.0368	0.0395
		HOSNT-15	0.0614	0.0720	0.0855	0.0305	0.0368	0.0395
5	1	HOSNT-9	0.2212	0.2524	0.2897	0.1133	0.1351	0.1440
		HOSNT-12	0.2192	0.2487	0.2840	0.1125	0.1341	0.1428
		HOSNT-15	0.2191	0.2486	0.2836	0.1125	0.1341	0.1426
	2	HOSNT-9	0.2225	0.2531	0.2897	0.1141	0.1361	0.1449
		HOSNT-12	0.2197	0.2485	0.2825	0.1133	0.1348	0.1433
		HOSNT-15	0.2196	0.2482	0.2819	0.1133	0.1348	0.1431
	3	HOSNT-9	0.2245	0.2550	0.2915	0.1154	0.1374	0.1462
		HOSNT-12	0.2211	0.2495	0.2829	0.1143	0.1360	0.1444
		HOSNT-15	0.2211	0.2492	0.2824	0.1143	0.1359	0.1443
	5	HOSNT-9	0.2262	0.2568	0.2930	0.1164	0.1368	0.1475
		HOSNT-12	0.2226	0.2506	0.2836	0.1153	0.1370	0.1454
		HOSNT-15	0.2225	0.2504	0.2831	0.1153	0.1370	0.1452

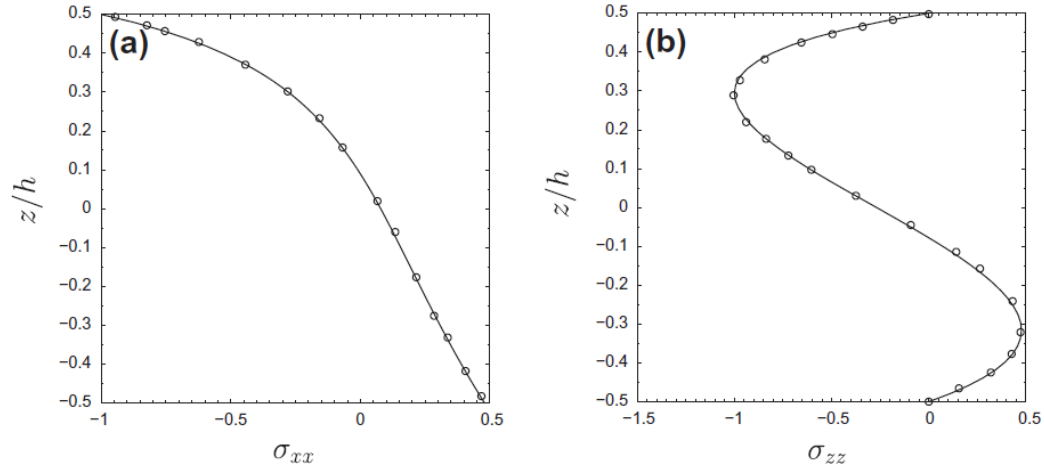

Figure 1

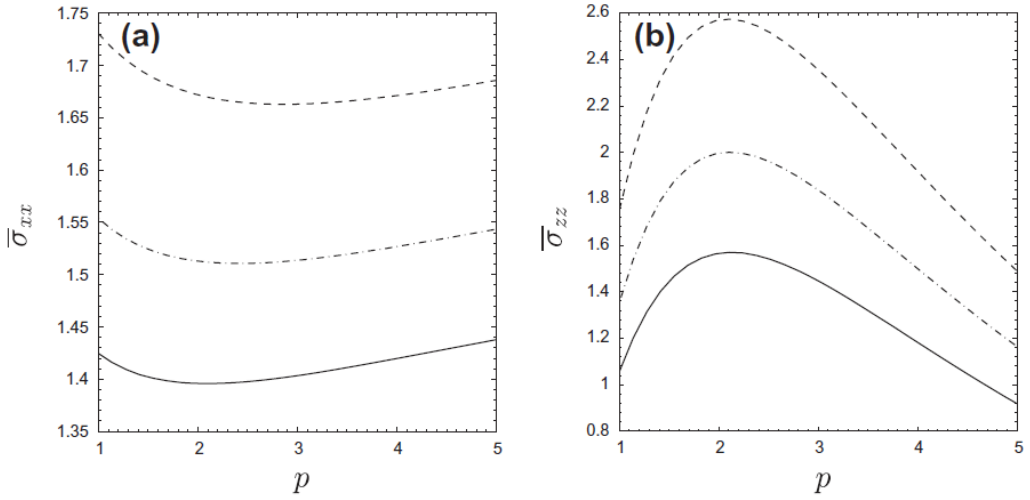

Figure 2

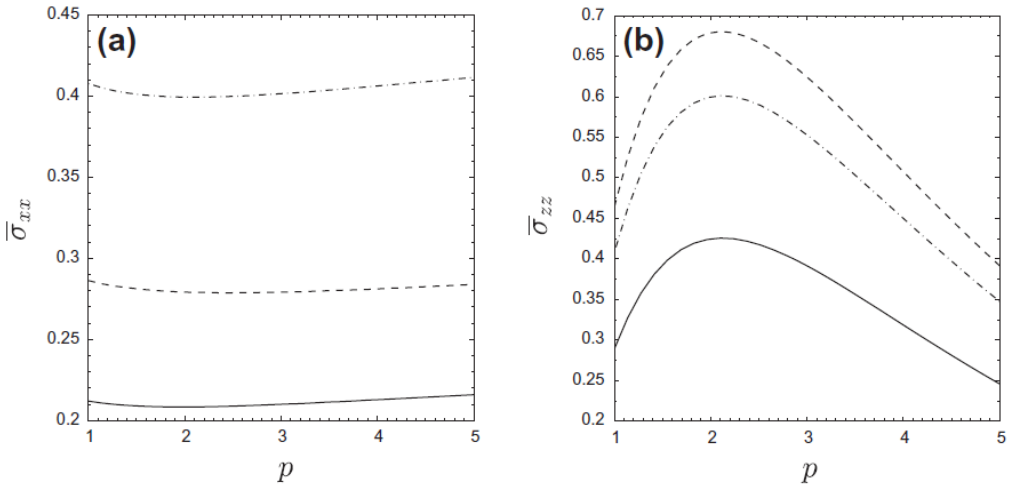

Figure 3